

Angular dependence of L x-ray production cross sections in uranium at 22.6- and 59.5-keV photon energies

D. Mehta,* Sanjiv Puri,† Nirmal Singh, M. L. Garg,‡ and P. N. Trehan
Department of Physics, Panjab University, Chandigarh 160 014, India

(Received 14 September 1998)

The Ll , $L\alpha$, $L\eta$, $L\beta_6$, $L\beta_{2,4}$, $L\beta_{1,3}$, $L\beta_{9,10}$, and $L\gamma$ x-ray production differential cross sections in ${}_{92}\text{U}$ have been measured using the 22.6- and 59.5-keV incident photon energies in an angular range 43° – 140° . The measurements were performed using the ${}^{109}\text{Cd}$ and ${}^{241}\text{Am}$ radioisotopes as photon sources and a Si(Li) detector. Differential cross sections for various L x rays are found to be angle independent within experimental error. This is contrary to the strong angular dependence of measured photon-induced Ll and $L\alpha$ x ray production cross sections as reported by Kahlon *et al.* [Phys. Rev. A **43**, 1455 (1991)] and M. Ertugrul [Nucl. Instrum. Methods Phys. Res. B **119**, 345 (1996)]. Integral cross sections for production of the Ll , $L\alpha$, $L\eta$, $L\beta_6$, $L\beta_{2,4}$, $L\beta_{1,3}$, $L\beta_{9,10}$, $L\gamma_{1,5}$, $L\gamma_{2,3,6}$, and $L\gamma_4$ x rays are also deduced in the present paper and are found to be in good agreement with those evaluated using the most reliable theoretical values of L_i ($i=1,2,3$) subshell photoionization cross sections, fluorescence yields, x-ray emission rates, and Coster-Kronig transition probabilities. [S1050-2947(99)09003-4]

PACS number(s): 32.80.Fb, 32.80.Hd

I. INTRODUCTION

Alignment of ionized atom resulting from photoionization of an inner shell by unpolarized radiation was first predicted by Flügge, Mehlhorn, and Schmidt [1] and Jacobs [2]. In the case where the angular momentum (J) of the resulting state of the ionized atom is $> \frac{1}{2}$, it is aligned, i.e., the relative population of different substates depends on the magnetic quantum number M_J , and is independent of its sign. Auger electrons or x rays emitted in the subsequent decay manifest this alignment through their anisotropic angular distribution or through polarization of the x rays. In a photoionization experiment [3–5] involving unpolarized incident beam and detection of x rays in singles mode, the state of the ion is axially symmetric about the incident beam direction and symmetric with respect to reflection in the plane perpendicular to the incident beam, and the angular distribution of emitted x rays is of the form $I(\Psi) = I_x[1 + \beta_2 P_2(\cos \psi)]$, where $P_2(\cos \psi)$ is the second-order Legendre polynomial. The coefficient of anisotropy is expressed as $\beta_2 = \alpha A_{20}$, where A_{20} is the degree of alignment and the coefficient α depends only on the J value of the initial and final states of ionized atom. Theoretical values of A_{20} for different states of various ionized atoms, calculated using wave functions obtained in the Herman-Skillman potential, have been reported by Berezhko, Kabachnik, and Rostovsky [6]. The values of the coefficient α are tabulated in [7].

Experimental investigations [8–16] of alignment of ionized atoms resulting from photoionization have been done

only in limited cases. The alignment of Kr^+ [8] and Xe^+ [9] ions with photon-induced vacancy in few states with $J \geq \frac{3}{2}$ has been investigated via angular distribution measurements of fluorescence radiations and Auger electrons, respectively. Similar studies in Cd^+ ions have been done via polarization measurements of fluorescence radiations [3,10]. Recently, Kahlon *et al.* [11–15] have investigated alignment of ionized atoms following L_i ($i=1,2,3$) subshell photoionization in some elements with $79 \leq Z \leq 92$. They have measured differential cross sections, $d\sigma(Lk)/d\Omega$, for production of Lk ($k=l, \alpha, \beta$, and γ) group of x rays at the 59.5-keV incident photon energy in the angular range $\psi = 40^\circ$ – 120° . The incident beam used in these measurements was unpolarized. The Ll and $L\alpha$ x rays originate from filling of the L_3 subshell ($J = \frac{3}{2}$) vacancies, the $L\gamma$ x rays from filling of the L_1 ($J = \frac{1}{2}$) and the L_2 ($J = \frac{1}{2}$) subshell vacancies and the $L\beta$ x rays from filling of all the three L_i subshell vacancies. The Ll and $L\alpha$ x-ray production cross sections were reported to exhibit strong and monotonous variation in the angular range covered in the measurements. The $L\beta$ and $L\gamma$ x-ray production cross sections were observed to be angle independent. Similar angular distribution results were reported by Kahlon [11] for different L x rays in case of Pb, Th, and U at the 25.8-keV incident photon energy. The Lk x ray production cross sections measured by Kahlon *et al.* [11–15] at the 59.5-keV incident photon energy were later on confirmed by Ertugrul [16]. Linear polarization measurements of the L x rays emitted following ionization by 59.5-keV photons in Th and U [11,12] have shown that the Ll and $L\alpha$ x rays are polarized, the $L\beta$ x rays are slightly polarized, and the $L\gamma$ x rays are unpolarized. From these investigations [11–16] it is concluded that the L_3 subshell vacancy state produced by photoionization is aligned whereas the L_1 and L_2 subshell vacancy states are not aligned.

The Ll and $L\alpha$ x-ray production cross sections measured by Kahlon *et al.* [11–15] and Ertugrul [16] are fitted to a polynomial in $\cos \psi$, which is equivalent to $I(\psi) = I_x[1$

*Present address: Department of Physics and Astrophysics, Delhi University, Delhi 110 007, India.

†Present address: Department of Physics, SLIET, Longowal 148 106, India.

‡Present address: Department of Biophysics, Panjab University, Chandigarh 160 014, India.

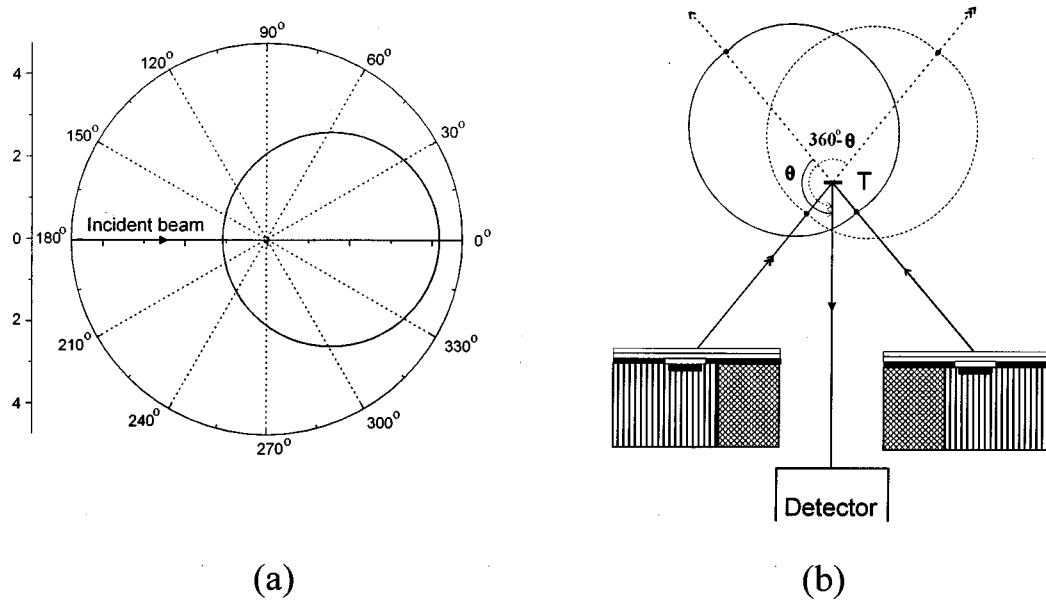


FIG. 1. (a) Polar plot depicting angular dependence of the L_1 x-ray production cross sections for uranium at the 59.5-keV incident photon energy. The plotted curve is generated from the polynomial in $\cos \psi$ fitted to differential cross sections measured by Kahlon *et al.* [11,12]. (b) Geometrical arrangement showing the measurement of L x-ray production cross sections corresponding to emission angle θ using photon source in the annular form symmetric about the direction of detected x rays. Polar plot of part (a) is also shown attached to the incident beam with target center T as origin. The differential cross sections corresponding to emission angles θ and $360^\circ - \theta$ are the same.

$+\kappa\beta_1P_1(\cos \psi)+\kappa\beta_2P_2(\cos \psi)$ involving both the odd- and even-order Legendre polynomials, where κ is a correction for transfer of unaligned vacancies from the L_1 and L_2 subshells to the L_3 subshell by Coster-Kronig transitions. The values of $\kappa\beta_1$ and $\kappa\beta_2$ in the case of the L_1 ($L\alpha$) x ray of

uranium, deduced from the work of Kahlon *et al.* [11,12], are 0.81 (1.47) and 0.24 (0.13), respectively, at the 25.8-keV incident photon energy and 0.71 (0.20) and 0.17 (-0.002), respectively, at the 59.5-keV incident photon energy. Large values of $\kappa\beta_1$ mean that angular dependence of the L_1 and

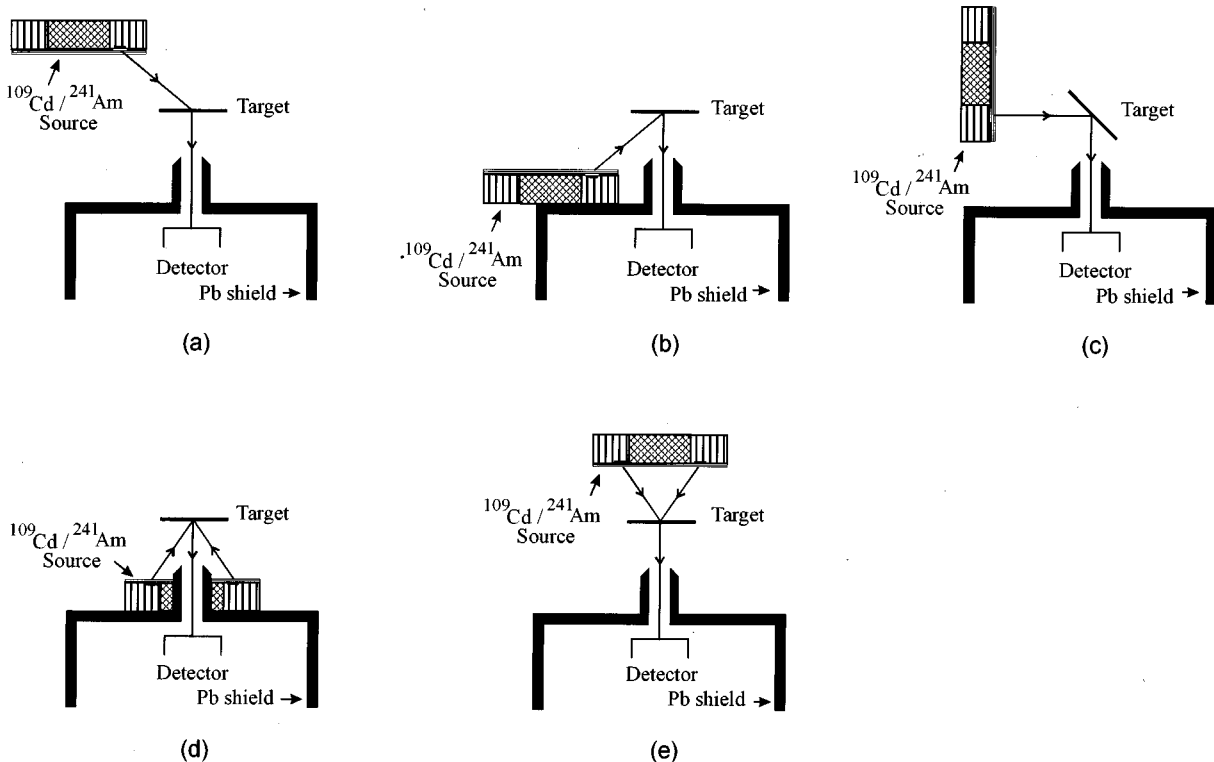


FIG. 2. Target, source, and detector geometrical setups used for the present measurements. Geometrical setups (a), (b), and (c) involve point source, and (c) and (d) involve annular source.

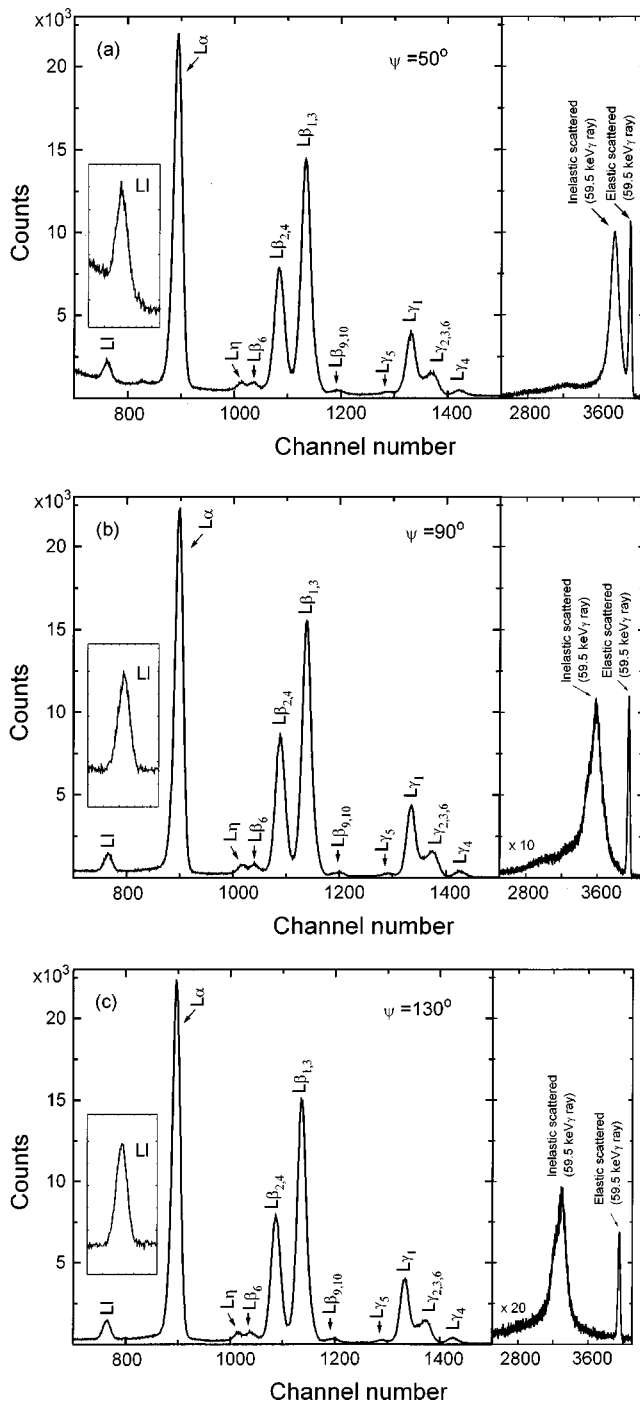


FIG. 3. Typical spectra of L x rays and scattered photons from the uranyl acetate target excited by the 59.5-keV photons from the ^{241}Am point source. The spectra taken corresponding to different ψ are normalized for the same area under the $L\gamma$ peak. Insets in (a) (c), showing $L\alpha$ x-ray part, have the same magnification.

$L\alpha$ x-ray production cross sections is strongly asymmetric with respect to reflection in the plane perpendicular to the incident beam [Fig. 1(a)]. As mentioned earlier in this section, the term involving $P_1(\cos \psi)$ is not expected in the polynomial fitted to cross sections measured in such an axially symmetric (noncoincident) photoionization experiment involving unpolarized incident beam [3–5]. In similar experiments [17–19] done using ion beams, the measured Ll and $L\alpha$ x-ray differential cross sections are fitted to poly-

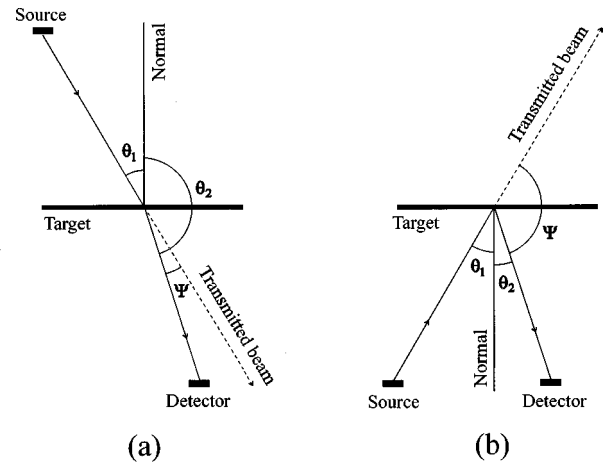


FIG. 4. (a) Transmission and (b) reflection geometrical setups used for differential x-ray production cross section measurements. Figures are redrawn to show geometrical variables.

mials involving $P_l(\cos \psi)$, $l=0,2$ only. An odd-order Legendre polynomial, $P_l(\cos \psi)$, is expected in the case where the incident photon beam is circularly polarized or in the ion-induced experiments having planar symmetry, e.g., where emitted x rays are observed in coincidence with the scattered incident ion [3]. Apart from this, certain inconsistencies are noticed in the earlier measured angular dependence of Ll and $L\alpha$ x ray production cross sections [11–15]. At the 25.8-keV incident photon energy, the reported anisotropy [$I(45^\circ)/I(105^\circ)$] for the $L\alpha$ group of x rays, consisting of the $L\alpha_1$ (L_3-M_5 , $\alpha=0.1$) [7] and $L\alpha_2$ (L_3-M_4 , $\alpha=-0.4$) [7] x rays of opposite anisotropy and with intensity ratio, $I(L\alpha_1)/I(L\alpha_2)\sim 9$, is even higher by a factor ~ 1.5 than that for the single Ll (L_3-M_1 , $\alpha=0.5$) [7] x ray in the case of U and the two are nearly the same in the case of Pb and Th [11]. At the 59.5-keV incident photon energy, anisotropy [$I(40^\circ)/I(120^\circ)$] for the $L\alpha$ x rays is smaller by factors 2.3, 1.7, and 1.3 than that observed in the Ll x ray in the case of Pb, Th, and U, respectively [11–13]. It may be added that theoretical calculations by Berezhko, Kabachnik, and Rostovsky [6] predict small values for the degree of alignment $A_{20}\sim 0.1$ for the L_3 subshell ionization at photon energy well above its binding energy, i.e., $\beta_2 < 0.05$ for Ll x ray. With these points in mind, it was felt necessary to reinvestigate the angular dependence of photon-induced L x-ray production cross sections.

In the present paper differential cross sections for production of the Ll , $L\alpha$, $L\eta$, $L\beta_6$, $L\beta_{2,4}$, $L\beta_{1,3}$, $L_{9,10}$, and $L\gamma$ x rays have been measured using the 22.6- and 59.5-keV incident photon energies, in the angular range 43° – 140° . A Si (Li) detector in vertical configuration and annular sources of ^{109}Cd and ^{241}Am , available with us, have been exploited to perform these measurements. The Ll , $L\alpha$, $L\eta$, $L\beta_6$, $L\beta_{2,4}$, $L\beta_{1,3}$, $L_{9,10}$, $L\gamma_{1,5}$, $L\gamma_{2,3,6}$, and $L\gamma_4$ x-ray production integral cross sections are also deduced and compared with the theoretical calculated ones [20]. It may be remarked that the 22.6- and 59.5-keV incident photon energies are below the K threshold of uranium ($E_K = 115.6$ keV), therefore, vacancies in the L_2 and L_3 subshells will be produced only through the Coster-Kronig transitions apart from the direct ionization. The vacancies transferred to the L_3 subshell from the L_1 and

TABLE I. Differential L x-ray production cross sections for uranium at the 59.5-keV incident photon energy. Error in measured values are given in the last row.

Emission angle (Ψ)	X-ray production cross sections (b/sr)								
	$d\sigma(Ll)/d\Omega$	$d\sigma(L\alpha)/d\Omega$	$d\sigma(L\eta)/d\Omega$	$d\sigma(L\beta_6)/d\Omega$	$d\sigma(L\beta_{2,4})/d\Omega$	$d\sigma(L\beta_{1,3})/d\Omega$	$d\sigma(L\beta_{9,10})/d\Omega$	$d\sigma(L\beta)/d\Omega$	$d\sigma(L\gamma)/d\Omega$
50°	1.90	32.5	0.61	0.66	11.0	23.8	0.36	36.4	8.75
68°	1.93	32.7	0.62	0.64	10.7	23.3	0.37	35.7	8.51
90°	1.97	32.4	0.62	0.68	11.0	23.1	0.39	35.9	8.59
112°	1.87	31.6	0.66	0.69	10.6	23.8	0.38	36.1	8.36
135°	1.96	32.7	0.63	0.64	10.8	23.4	0.38	36.0	8.59
125° ^a	1.87	31.1	0.62	0.66	10.6	22.9	0.37	35.2	8.43
Error	0.17	2.3	0.07	0.08	0.8	1.7	0.04	2.5	0.70

^aMeasurements done using ²⁴¹Am annular source and 188- $\mu\text{g}/\text{cm}^2$ UF₄ target.

L_2 subshells ($J = \frac{1}{2}$) through Coster-Kronig transitions will not be aligned. The number of vacancies produced in the L_3 subshell due to direct ionization and through Coster-Kronig transitions, estimated using theoretical values of photoionization cross sections [21] and Coster-Kronig transition probabilities [22], are in the ratio 2.7:1.0 and 1.2:1.0 at the 22.6- and 59.5-keV incident photon energies, respectively.

II. EXPERIMENTAL DETAILS

A. Experimental procedure

The L x-ray differential cross-section measurements have been done using photon sources in the annular form as well as the point form. For measurements using the ¹⁰⁹Cd and ²⁴¹Am point sources, the geometrical setups shown in Figs. 2(a)–2(c) were used. The ²⁴¹Am (2Ci) and ¹⁰⁹Cd (5 m Ci) sources, both procured from Dupont, U.S., are in the form of a circular flat ribbon of 30-mm diameter and 4-mm width. The ²⁴¹Am source was covered with Pb mask (1.4 g/cm² thick Pb in annular shape with a hole) to convert it to a point source of dimensions 5 mm \times 4 mm. This arrangement was further covered with Cu-Al-graded absorber (0.3 g/cm² thick Cu and 0.1 g/cm² thick Al) to absorb the 26.3-keV γ -ray and the Np L x rays from the unmasked portion of ²⁴¹Am source, and the Pb L x rays from the mask. This arrangement has been used as a 59.5-keV photon point source. Similarly, the ¹⁰⁹Cd source covered with a Pb-Al-graded mask has been used as a 22.6-keV photon point source. The average energy of Ag-K x rays emitted from ¹⁰⁹Cd source was calculated to be 22.6 keV by considering the weighted average of the energies of Ag $K\alpha$ and $K\beta$ x ray in proportion to their intensity values [23]. The 88.2-keV γ -rays from whole of the ¹⁰⁹Cd annular source, being partially absorbed in the Pb-Al mask, also fall on the target. The measured cross sections have been corrected for a small contribution due to these γ -rays. A Si(Li) detector [28.27 mm² \times 5.5 mm, Be window thickness=0.0254 mm and full width at half maximum (FWHM)=200 eV at 5.89 keV] in vertical configuration was used to detect x rays emitted from target. The detector was placed in a Pb housing to minimize detection of radiations coming directly from the source and those scattered from the surroundings. A 5-mm diameter Pb collimator was used in front of the detector. The Pb housing and collimator were lined from inside with Al. The whole arrangement resulted in

a smooth background in the energy region above 8 keV. The L x-ray production differential cross-section measurements corresponding to forward emission angles ($\psi < 90^\circ$) were performed using the transmission geometry [Fig. 2(a)] and those corresponding to backward emission angles ($\psi < 90^\circ$) were performed using the reflection geometry [Fig. 2(b)]. For measurements corresponding to the 90° emission angle, the reflection geometry shown in Fig. 2(c) was used. In this geometry, the target makes a 45° angle with the incident and detected photon beams and the target-to-detector distance is the same as in the geometrical setups shown in Figs. 2(a) and 2(b). For differential cross section measurements using the ¹⁰⁹Cd and ²⁴¹Am annular sources, the geometrical setups shown in Figs. 2(d) and 2(e) were used. The strongly asymmetric angular dependence of production cross sections for the Ll and $L\alpha$ x rays [Fig. 1(a)] as reported by Kahlon *et al.* [11–15] using point-source geometry is also expected to be

TABLE II. L x-ray production differential cross sections for uranium at the 22.6-keV incident photon energy. Error in measured values are given in separate rows.

Emission angle (Ψ)	X-ray production cross sections (b/sr)				
	$d\sigma(Ll)/d\Omega$	$d\sigma(L\alpha)/d\Omega$	$d\sigma(L\beta_{2,4})/d\Omega$	$d\sigma(L\beta_{1,3})/d\Omega$	$d\sigma(L\beta)/d\Omega$
Using ¹⁰⁹ Cd annular source:					
50°	24.4	404	113	293	423
60°	25.0	404	113	294	424
70°	25.0	404	117	304	438
100°	24.0	390	110	287	414
120°	24.4	407	115	299	431
140°	24.0	404	116	301	433
Error	2.4	27	9	22	29
Using ¹⁰⁹ Cd point source:					
43°	24	408	109	285	410
54°	27	410	106	276	398
67°	28	450	116	301	434
102°	22	409	110	285	410
125°	26	408	110	285	410
130°	24	396	108	281	405
Error	4	36	11	27	37

observed in the measurements done using annular-source geometry [see Fig. 1(b)]. The annular-source geometry has also been used by various workers [24–26] to measure elastic scattering differential cross sections for low-energy photons, which are also expected to be axially symmetric about the incident beam direction and strongly asymmetric with respect to reflection in the plane perpendicular to the incident beam.

Spectroscopically pure targets of 12.7-mg/cm^2 uranyl acetate [$\text{UO}_2(\text{CH}_3\text{COO})_2 \cdot 2\text{H}_2\text{O}$], (prepared by pressing powder between two $2\text{-}\mu\text{m}$ Mylar layers) and $188\text{-}\mu\text{g/cm}^2$ UF_4 on $6\text{-}\mu\text{m}$ Mylar backing (Micromatter Inc., USA) were used. The L x-ray spectra were taken (i) using the uranyl acetate target and the ^{241}Am point source, (ii) using the UF_4 target and the ^{109}Cd annular source, (iii) using the UF_4 target and the ^{109}Cd point source, and (iv) using the uranyl acetate target and the ^{109}Cd point source. A PC-based multichannel analyser (Canberra, Model S-100) has been used for acquisition of these spectra. To reduce statistical error in the above mentioned measurements (i)–(iv), the spectra were recorded for total times of 25 h, 15 h, 100 h, and 12 h, respectively, at each angle. The integral count rate in the Si(Li) detector was less than 400 cps in all the measurements. It ensured stability of the system and avoided deterioration of spectrum due to random summing effects. Typical spectra from the uranyl acetate target, excited by 59.5-keV photons from the ^{241}Am point source, corresponding to $\Psi = 50^\circ$, 90° , and 130° are shown in Figs. 3(a)–(c), respectively. Each spectrum shows well-resolved groups of the Ll , $L\alpha$, $L\eta$, $L\beta_6$, $L\beta_{2,4}$, $L\beta_{1,3}$, $L\beta_{9,10}$, $L\gamma_{1,5}$, $L\gamma_{2,3,6}$, and $L\gamma_4$ x ray lines of uranium. In the case of spectra taken at the 22.6-keV incident photon energy, the uranium $L\gamma$ x-ray peak overlaps with the peak corresponding to inelastic scattered $\text{Ag } K\alpha$ x-ray. The energy shift of the inelastic scattered peak from the elastic scattered peak in spectrum from a low- Z Al target was used as a tool to define the angle of incidence in different geometrical set-ups used in the present measurements. Further, computer-based simulations were used to estimate the angular spread in the emission angle of the detected L x rays. The shape of the angular spread is nearly Gaussian with $\text{FWHM} \sim 10^\circ$ (see Fig. 3 of [24]).

B. Evaluation procedure

The measured differential cross sections (cm^2/g) for Lk x rays were evaluated using the equation

$$\frac{d\sigma(Lk)}{d\Omega} = \frac{N_{Lk}}{4\pi I_0 G \varepsilon_{Lk} m \beta_{Lk}}, \quad (1)$$

where N_{Lk} is the number of counts/s under the Lk x-ray peak, $I_0 G$ is intensity of photons falling on the portion of target

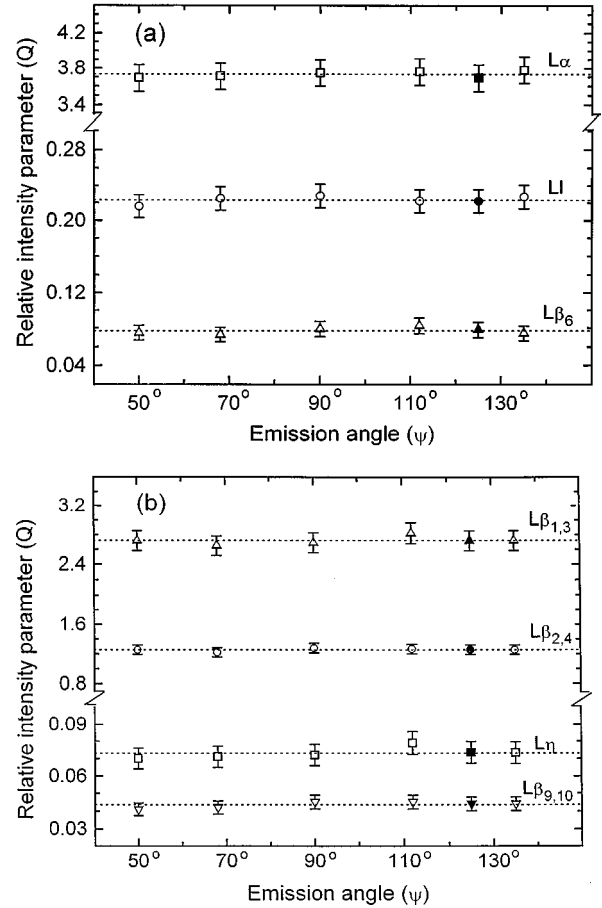


FIG. 5. Relative intensity parameter Q for different L x rays as a function of emission angle ψ measured at the 59.5-keV incident photon energy. Open and filled symbols correspond to measurements done using ^{241}Am source in point and annular form, respectively. Dotted line corresponds to the average value.

visible to the detector, ε_{Lk} is the detector efficiency at Lk x-ray energy, m is the mass thickness of uranium in the target in g/cm^2 , and β_{Lk} is the absorption-correction factor that accounts for absorption of the incident photons and the emitted Lk x ray in the target. The cross sections were converted to barns/atom units using the factor given in [27]. The values of β_{Lk} have been calculated using Eqs. (2) and (3) for the reflection and transmission geometrical setups, respectively.

$$\beta = \frac{1 - \exp\left[-\sum_i \{(\mu/\rho)_{1i}/\cos\theta_1 + (\mu/\rho)_{2i}/\cos\theta_2\} m_i\right]}{\sum_i \{(\mu/\rho)_{1i}/\cos\theta_1 + (\mu/\rho)_{2i}/\cos\theta_2\} m_i}, \quad (2)$$

$$\beta = \exp\left[\sum_i (\mu/\rho)_{2i} m_i / \cos\theta_2\right] \frac{1 - \exp\left[-\sum_i [(\mu/\rho)_{1i}/\cos\theta_1 + (\mu/\rho)_{2i}/\cos\theta_2] m_i\right]}{\sum_i [(\mu/\rho)_{1i}/\cos\theta_1 + (\mu/\rho)_{2i}/\cos\theta_2] m_i}, \quad (3)$$

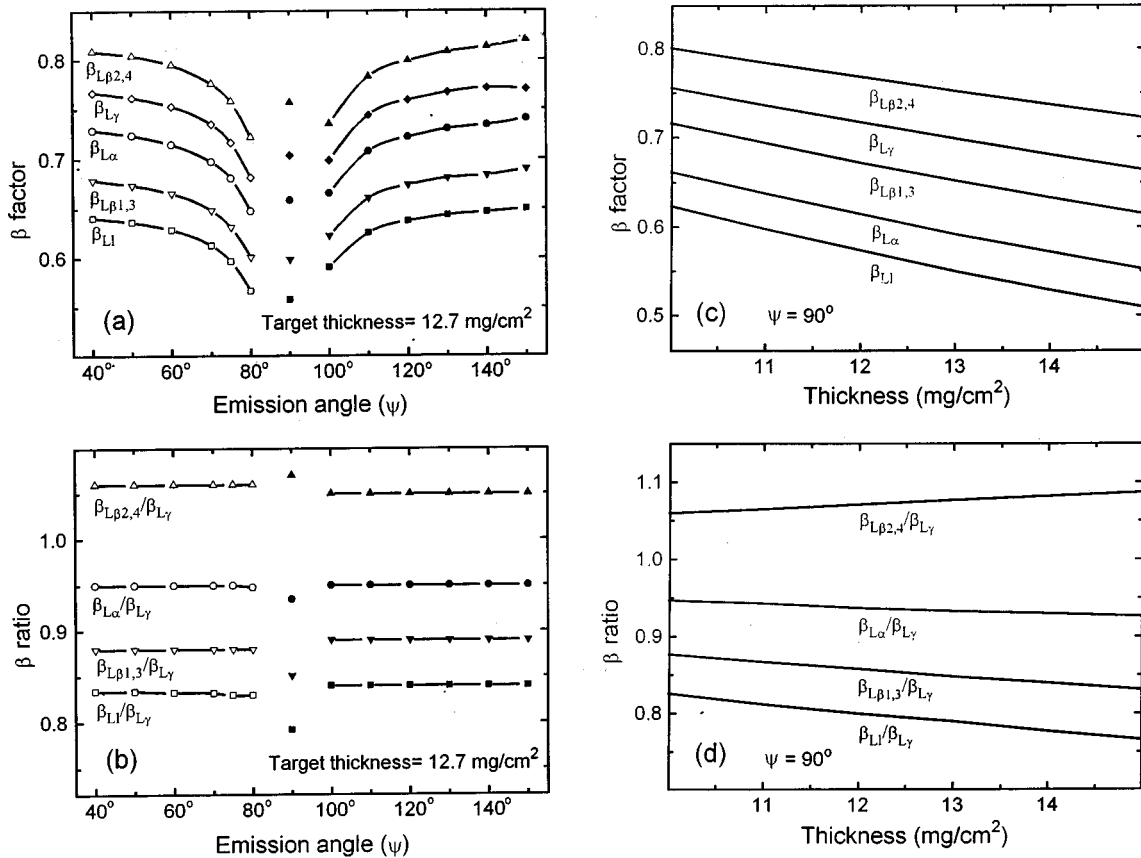


FIG. 6. Absorption-correction factor $\beta(Lk)$ and the ratios $\beta(Lk)/\beta(L\gamma)$ for different L x rays in the case of the uranyl acetate target and the 59.5-keV incident photon energy are plotted in (a) and (b), respectively, as a function of emission angle (Ψ), and in (c) and (d), respectively, as a function of target thickness. Filled and open symbols in (a) and (b) correspond to reflection and transmission geometrical setups, respectively.

where summation over i stands for different elements present in the compound target. $(\mu/\rho)_{1i}$ and $(\mu/\rho)_{2i}$ are attenuation coefficients corresponding to the incident and emitted photon energies, respectively, in i th element present in the target and were taken from the tables of Hubbell and co-workers [28,29]. θ_1 and θ_2 are angles, which the incident and emitted photons make with the positive normal to target (Fig. 4).

To determine the number of counts/s under the Lk x ray peak N_{Lk} , each spectrum was analyzed for photopeak areas using a computer code PEAKFIT [30,31]. In this code, a non-linear least-squares fitting routine, involving fitting of multi-Gaussian function plus polynomial background, is used. The $I_0G\epsilon$ values corresponding to the 22.6- and 59.5-keV incident photons were determined over the energy range 7–21 keV and 7–30 keV, respectively, by measuring the K x ray yields from spectroscopically pure targets of Ni, Cu, Zn, Ge, Se, SrF₂, YF₃, Nb₂O₃, MoO₃, Rh, Pd, Ag, In, Sn, and BaF₂ (thickness 100–300 $\mu\text{g}/\text{cm}^2$, Micromatter, USA) and using the knowledge of theoretical K x-ray production cross sections [20]. The details are given elsewhere [24,31]. The product $I_0G\epsilon_{Lk}$ corresponding to the Lk x-ray energy was used in Eq. (1).

III. RESULTS AND DISCUSSION

The $L1$, $L\alpha$, $L\eta$, $L\beta_6$, $L\beta_{2,4}$, $L\beta_{1,3}$, $L\beta_{9,10}$, and $L\gamma$ x ray differential cross sections in uranium at the 59.5-keV

incident photon energy, measured using the uranyl acetate target and the ^{241}Am point source, are listed in Table I. The $L1$, $L\alpha$, $L\beta_{1,3}$, and $L\beta_{2,4}$ x-ray differential cross sections in uranium at the 22.6-keV incident photon energy, measured using thin UF₄ target and the ^{109}Cd source in point form as well as annular form, are listed in Table II. Differential cross sections for the weak $L\eta$, $L\beta_6$, and $L\beta_{9,10}$ x rays at the 22.6-keV incident photon energy are not being reported due to low statistics. The percentage error in the measured cross sections is attributed to uncertainties in different parameters used in Eq. (1), namely, error in evaluation of photopeak areas ($\sim 3\%$ for strong and well-separated peaks and up to 10% for weak components separated using fitting procedures), in the attenuation coefficients used to evaluate β_{Lk} (4%), in uniformity of target (5%), and in evaluation of the $I_0G\epsilon_{Lk}$ factor (5%). The error in evaluation of L x-ray photopeak areas in the spectra taken using thin UF₄ target and the ^{109}Cd point source is 5–15% due to low statistics and poor peak-to-background ratio. It is clear from Tables I and II that the x-ray production differential cross sections for various L x-rays measured at different angles match within experimental error at both the 22.6- and 59.5-keV incident photon energies. Differential cross sections measured using the ^{109}Cd point source agree with those measured using the ^{109}Cd annular source (Table II).

The $L\gamma$ group of x rays, being emitted following the decay of L_1 ($J = \frac{1}{2}$) and L_2 ($J = \frac{1}{2}$) subshell vacancies, is ex-

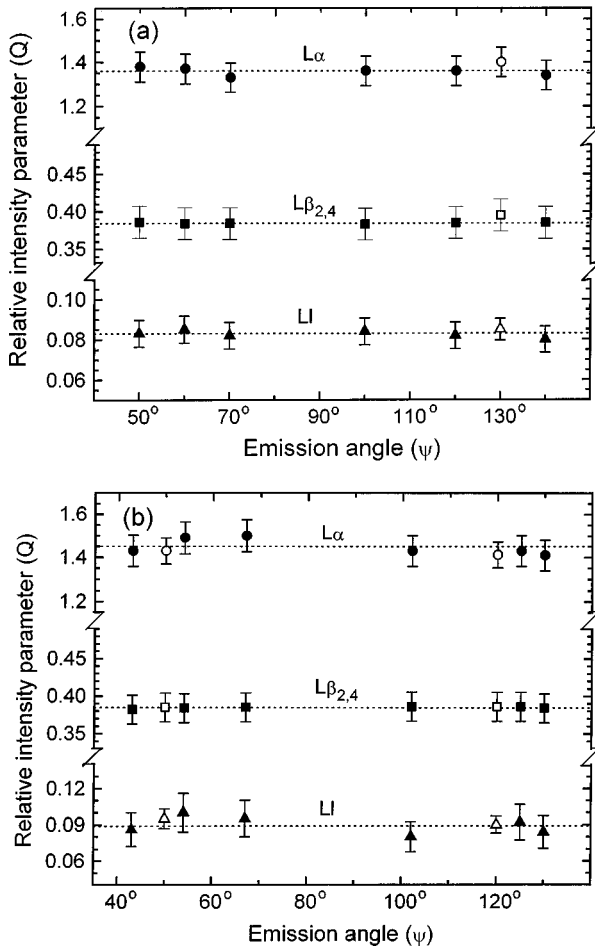


FIG. 7. Relative intensity parameter Q for the $L1$, $L\alpha$, and $L\beta_2$ x rays as a function of emission angle ψ measured at the 22.6-keV incident photon energy; (a) using ^{109}Cd annular source, and (b) using ^{109}Cd point source. Filled and open symbols correspond to measurements done using thin UF_4 and thick uranyl acetate targets, respectively. Dotted line corresponds to the average value.

pected to exhibit isotropic emission; $\alpha=0$ in the case where the initial vacancy state is $J=\frac{1}{2}$ [7]. Therefore, angular dependence of differential cross sections for Lk x ray can be borne out confidently by plotting the relative intensity parameter $Q(Lk) = (N_{Lk}\beta_{L\gamma}\varepsilon_{L\gamma}) / (N_{L\gamma}\beta_{Lk}\varepsilon_{Lk})$ for different x ray emission angles ψ . This parameter represents the intensity of the Lk x ray relative to the $L\gamma$ group of x rays. The parameter Q for different L x rays at the 59.5-keV incident photon energy is plotted in Fig. 5, for different emission angles ψ . It is clear from this plot that emission of all the L x rays, including the $L1$, $L\alpha$, and $L\beta_6$ x rays originating purely from the decay of the L_3 subshell vacancies ($J=\frac{3}{2}$), is isotropic within experimental error. It is worth mentioning that $\mu_1 \ll \mu_2$ for the L x-ray emission at the 59.5-keV incident photon energy, e.g., $\mu_1 = 3.93 \text{ cm}^2/\text{gm}$ [27] and $\mu_2 = 58.9 \text{ cm}^2/\text{gm}$ [27] for the $L\beta_1$ x ray emitted from the uranyl acetate target. For the 12.7-mg/cm² thick uranyl acetate target, β_{Lk} values are plotted in Fig. 6(a) for emission angles in the range 40°–70° in the transmission geometry [Fig. 2(a)], in the range 100°–140° in the reflection geometry [Fig. 2(b)], and for the 90° emission angle in the reflection geometry [Fig. 2(c)]. It shows nearly the same values of β_{Lk} over the emission angles involved in the present measurements.

Also, the β_{Lk} factors exhibit weak dependence on target thickness [Fig. 6(c)] in the vicinity of the thickness = 12.7 mg/cm² used in the present paper. The ratio $\beta_{Lk}/\beta_{L\gamma}$, directly involved in determination of $Q(Lk)$, is found to be nearly constant with ψ [Fig. 6(b)] as well as target thickness [Fig. 6(d)]. Also, the detector efficiency ratio, $\varepsilon_{L\gamma}/\varepsilon_{Lk}$, is the same in measurements corresponding to different ψ because of the same position of the target with respect to the detector in different geometrical setups used. Therefore, the angular dependence of parameter $Q(Lk)$ is mainly determined by the peak area ratio, $N_{Lk}/N_{L\gamma}$, in the spectra taken at different ψ . Further, to look for anisotropy in emission of the $L\alpha_2$ x ray, measurements were done using the ^{241}Am point source and the uranyl acetate target, and by placing the KBr absorber (thickness = 27.0 mg/cm², prepared by soaking KBr aqueous solution onto filter paper), at the collimator end close to the Si(Li) detector. Br has K-shell binding energy of 13.474 keV and the jump ratio = 6.974 [27]. This arrangement reduced the $U-L\alpha_1$ x-ray (13.618 keV) count rate to ~5% while the $U-L\alpha_2$ x-ray (13.442 keV) count rate is reduced to ~50%, thereby changing the $N_{L\alpha_1}/N_{L\alpha_2}$ ratio considerably (from ~9 without absorber to ~1 with absorber) in the composite peak. The measurements done for $\psi=50^\circ$ and 130° using the ^{241}Am point source and for $\psi=130^\circ$ using the ^{241}Am annular source, give fairly constant values of the parameter Q (without correction for absorption in the KBr absorber) for the $L\alpha$, $L\beta_{2,4}$, and $L\beta_{1,3}$ x rays. In these spectra, the $U-L1$ x-ray peak overlaps with the Br $K\alpha$ x-ray peak. These measurements indicate that emission of the $L\alpha_2$ x-ray is also isotropic within experimental error.

At the 22.6-keV incident photon energy, the relative intensity parameter $Q(Lk)$ has been defined as $(N_{Lk}\beta_{L\beta_{1,3}}\varepsilon_{L\beta_{1,3}}) / (N_{L\beta_{1,3}}\beta_{Lk}\varepsilon_{Lk})$, i.e., using the $L\beta_{1,3}$ group of x rays instead of the $L\gamma$ x ray used in case of the 59.5-keV incident photon energy. The $L\beta_{1,3}$ group of x rays, mainly resulting from decay of the L_1 ($J=\frac{1}{2}$) and L_2 ($J=\frac{1}{2}$) subshell vacancies, is also expected to exhibit isotropic emission. The peak corresponding to the $L\beta_{1,3}$ x rays is well resolved and the fractional contribution of the $L\beta_5$ x ray ($L_3-O_{4,5}$) to this peak is only ~0.05. The parameter Q for the $L1$, $L\alpha$, and $L\beta_{2,4}$ x-rays measured using thin UF_4 target and the ^{109}Cd source in annular form and point form are plotted in Figs. 7(a) and 7(b), respectively, for different ψ . The values of parameter Q for these x rays corresponding to different ψ are constant within experimental error. The β_{Lk} correction in the case of the UF_4 target used is small ($\beta_{Lk} \geq 0.98$). Therefore, the angular dependence of parameter Q in these measurements is also mainly determined by the peak area ratio, $N_{Lk}/N_{L\beta_{1,3}}$. The values of the parameter Q for these L x rays determined from the measurements done using uranyl acetate target, and the ^{109}Cd source in annular form and point form are also found to be consistent [Figs. 7(a) and 7(b)].

In similar measurements for Pb and Th at the 59.5-keV incident photon energy, the values of relative intensity parameter Q for the $L1$, $L\alpha$, and $L\beta$ x rays are also found to be constant in the angular range 50°–130°. These observations clearly contradict the strong anisotropy in emission of the $L1$ and $L\alpha$ x rays, as reported by Kahlon *et al.* [11–15] and

TABLE III. L x-ray production integral cross sections for uranium element at the 22.6- and 59.5-keV incident photon energies. Error in measured values are given in parentheses.

X-ray production cross sections (barns/atom)				
X-ray	At 22.6-keV excitation energy		At 59.5-keV excitation energy	
	Measured	Calculated	Measured	Calculated
$L1$	307(25)	315	24.1(20)	24.0
$L\alpha$	5060(35)	5022	403(25)	382
$L\eta$	105(12)	94	7.9(7)	7.3
$L\beta_6$	102(13)	80	8.3(9)	6.1
$L\beta_{2,4}$	1434(10)	1338	135(10)	120
$L\beta_{1,3}$	3730(290)	3703	293(21)	305
$L\beta_{9,10}$	25(3)	28	4.71(42)	4.32
$L\beta$	5396(376)	5243	449(30)	435
$L\gamma_{1,5}$	901(72)	802	65.6(45)	60.7
$L\gamma_{2,3,6}$	-	290	34.0(26)	32.6
$L\gamma_4$	-	32.5	5.9(5)	4.9
$L\gamma$	-	1123	106(7)	100

Ertugrul [16]. It may be added that the experimental and evaluation procedures adopted for the L x-ray cross-section measurements in the present paper and by Kahlon *et al.* [11–15] and Ertugrul [16] are the same. Further, we have also reported the measured Lk ($k = \alpha, \beta,$ and γ) x-ray production cross sections for elements with $56 \leq Z \leq 92$ at various incident photon energies ranging 10–60 keV [32–35]. These measurements were done using annular sources of ^{241}Am and ^{109}Cd radioisotopes in the direct excitation mode ($\Psi = 114^\circ$ [36]) and in the secondary excitation mode ($\Psi = 148^\circ$ [36]) using secondary excitors of Se, Y, Mo, Ag, Sn, and Dy elements in conjunction with the ^{241}Am annular source. None of the measurements [32–35] evidenced such a strong angular dependence of the Ll and $L\alpha$ x-ray production cross sections as reported by Kahlon *et al.* [11–15] and by Ertugrul [16]. The measured integral cross sections [32–35], calculated assuming isotropic emission of the L x-rays, were observed to be in general agreement with the theoretical ones [20,32–35].

In conclusion, our measurements indicate, contrary to other recently reported results, that emission of the $Ll, L\alpha, L\eta, L\beta_6, L\beta_{2,4}, L\beta_{1,3}, L\beta_{9,10},$ and $L\gamma$ x rays in the case of U, following ionization at both the 59.5- and 22.6-keV photon energies, is isotropic within experimental error. More precise experimental studies are required to observe the predicted small anisotropy ($A_{20} \sim 0.1$) [6] in the emission of L x rays subsequent to decay of the photon-induced L_3 subshell vacancies. The incident photon energy should be chosen such that $E_{L_3} < E_{\text{inc}} < E_{L_2}, E_{L_i}$ being the L_i subshell binding

energy. This will eliminate reduction in the observed anisotropy due to the transfer of unaligned L_1 and L_2 subshell vacancies to the L_3 subshell through Coster-Kronig transitions, i.e., $\kappa = 1$.

In view of the above-established isotropic nature of the emission of different L x rays, the L x-ray production integral cross sections were determined by multiplying the average of differential cross sections measured at various angles by a factor of 4π . Further, all the spectra taken at the 22.6-keV incident photon energy were added and analyzed for the weak $L\eta, L\beta_6$ and $L\beta_{9,10}$ x rays using fitting procedures [30,31]. The $L\gamma_{1,5}$ x-ray cross sections were determined from the spectra taken at forward angles, where this x-ray peak can be easily separated from the inelastic scattered Ag $K\alpha$ peak. The theoretical cross sections calculated using the L_i subshell photoionization cross sections based on the Dirac-Hartree-Slater model [21], L_i subshell fluorescence yields and Coster-Kronig transition probabilities based on the relativistic Dirac-Hartree-Slater model [22,37] and x ray emission rates based on the Dirac-Fock model [38], are also given in Table III. The details of calculations are given elsewhere [20,31]. The measured results are found to be in general agreement with the theoretical ones.

ACKNOWLEDGMENTS

Financial support from the University Grants Commission, New Delhi, in the form of Center of Advance Study Funds, and from the Department of Science and Technology, New Delhi, is duly acknowledged.

[1] S. Flügge, W. Mehlhorn, and V. Schmidt, Phys. Rev. Lett. **29**, 7 (1972).

[2] V. L. Jacobs, J. Phys. B **5**, 2257 (1972).

[3] W. Mehlhorn, in *X-ray and Atomic Inner-shell Physics*, edited

by B. Crasemann, AIP Conf. Proc. No. 94 (AIP, New York, 1982) p. 53.

[4] W. Jitschin, in *X-ray and Atomic Inner-shell Physics* (Ref. [3]), p. 74.

- [5] B. Cleff, *Acta Phys. Pol. A* **61**, 285 (1982).
- [6] E. G. Berezhko, N. M. Kabachnik, and V. S. Rostovsky, *J. Phys. B* **11**, 1749 (1978).
- [7] E. G. Berezhko and N. M. Kabachnik, *J. Phys. B* **10**, 2467 (1977).
- [8] H. Schmoranzner, S. Lauer, F. Vollweiler, A. Ehresmann, V. L. Sukhorukov, B. M. Lagutin, I. V. Petrov, Ph. V. Demekhin, K.-H. Schartner, B. Magel, and G. Mentzel, *J. Phys. B* **30**, 4463 (1997).
- [9] S. H. Southworth, P. H. Kobrin, C. M. Truesdale, D. Lindle, S. Owaki, and D. Shirley, *Phys. Rev. A* **24**, 2257 (1981).
- [10] C. D. Caldwell and R. N. Zare, *Phys. Rev. A* **16**, 255 (1977).
- [11] K. S. Kahlon, Ph.D. thesis, Punjabi University, Patiala, India, 1991 (unpublished).
- [12] K. S. Kahlon, H. S. Aulakh, N. Singh, R. Mittal, K. L. Allawadhi, and B. S. Sood, *Phys. Rev. A* **43**, 1455 (1991).
- [13] K. S. Kahlon, K. Shatendra, K. L. Allawadhi, and B. S. Sood, *J. Phys. B* **23**, 2733 (1990).
- [14] K. S. Kahlon, K. Shatendra, K. L. Allawadhi, and B. S. Sood, *Pramana* **35**, 105 (1990).
- [15] K. S. Kahlon, N. Singh, R. Mittal, K. L. Allawadhi, and B. S. Sood, *Phys. Rev. A* **44**, 4379 (1991).
- [16] M. Ertugrul, *Nucl. Instrum. Methods Phys. Res. B* **119**, 345 (1996).
- [17] T. Papp and B. Schlenk, *J. Phys. B* **20**, 2255 (1987).
- [18] T. Papp and J. Palinkas, *Phys. Rev. A* **38**, 2686 (1988).
- [19] A. P. Jesus, J. P. Ribeiro, I. B. Niza, and J. S. Lopes, *J. Phys. B* **22**, 65 (1989).
- [20] S. Puri, B. Chand, D. Mehta, M. L. Garg, N. Singh, and P. N. Trehan, *At. Data Nucl. Data Tables* **61**, 289 (1995).
- [21] J. H. Scofield, Lawrence Livermore Laboratory Report No. UCRL-51 326, 1973 (unpublished).
- [22] S. Puri, D. Mehta, B. Chand, N. Singh, and P. N. Trehan, *X-Ray Spectrom.* **22**, 358 (1993).
- [23] E. Browne and R. B. Firestone, in *Table of Radioactive Isotopes*, edited by V. S. Shirley (Wiley, New York, 1986).
- [24] J. S. Shahi, S. Puri, D. Mehta, M. L. Garg, N. Singh, and P. N. Trehan, *Phys. Rev. A* **55**, 3557 (1997); **57**, 4327 (1998).
- [25] K. M. Varier and M. P. Unnikrishanan, *Nucl. Instrum. Methods Phys. Res. A* **280**, 428 (1989).
- [26] G. Basavaraju, P. P. Kane, S. M. Lad, L. Kissel, and R. H. Pratt, *Phys. Rev. A* **51**, 2608 (1995).
- [27] E. Storm and I. Israel, *Nucl. Data, Sect. A* **7**, 565 (1970).
- [28] J. H. Hubbell and S. M. Seltzer, National Institute of Standards and Technology Report No. NISTIR 5632, 1995 (unpublished).
- [29] D. E. Cullen, J. H. Hubbell, and L. Kissel, Lawrence Livermore National Laboratory Report No. EPDL97, UCRL-50 400, Vol. 6, Rev. 5, 1997 (unpublished).
- [30] J. Singh, R. Singh, D. Mehta, N. Singh, and P. N. Trehan, *Nucl. Phys. B* **37**, 455 (1995).
- [31] S. Puri, D. Mehta, N. Singh, and P. N. Trehan, *Phys. Rev. A* **54**, 617 (1996).
- [32] S. Singh, D. Mehta, M. L. Garg, S. Kumar, N. Singh, and P. N. Trehan, *J. Phys. B* **20**, 3325 (1987).
- [33] S. Singh, D. Mehta, M. L. Garg, N. Singh, and P. N. Trehan, *J. Phys. B* **22**, 1163 (1989).
- [34] S. Singh, D. Mehta, R. R. Garg, S. Kumar, M. L. Garg, N. Singh, J. H. Hubbell, and P. N. Trehan, *J. Phys. B* **20**, 5345 (1987).
- [35] S. Singh, D. Mehta, S. Kumar, M. L. Garg, N. Singh, P. C. Mangal, and P. N. Trehan, *X-Ray Spectrom.* **18**, 193 (1989).
- [36] M. L. Garg, J. Singh, H. R. Verma, N. Singh, P. C. Mangal, and P. N. Trehan, *J. Phys. B* **17**, 577 (1984).
- [37] M. H. Chen, B. Crasemann, and H. Mark, *Phys. Rev. A* **24**, 177 (1981).
- [38] J. L. Campbell and J. X. Wang, *At. Data Nucl. Data Tables* **43**, 281 (1989).